WIND ENERGY
Wind Energ. (2009)
Published online in Wiley Interscience
(www.interscience.wiley.com) DOI: 10.1002/we.326

Research Article

A Dynamic Stall Model for Airfoils with Deformable Trailing Edges

Peter Bjørn Andersen, **Mac Gaunaa**, **Christian Bak and Morten Hartvig Hansen**, Risø-DTU, VEA, Roskilde, Denmark

Key words:
trailing-edge flaps;
dynamic stall;
shed vorticity model;
unsteady
aerodynamics;
smart material

The present work contains an extension of the Beddoes–Leishman-type dynamic stall model. In this work, a deformable trailing-edge flap has been added to the dynamic stall model. The model predicts the unsteady aerodynamic forces and moments on an airfoil section undergoing arbitrary motion in heave, lead-lag, pitch, trailing-edge flapping. In the linear region, the model reduces to the inviscid model, which includes the aerodynamic effect of a thin airfoil with a deformable camberline in inviscid flow. Therefore, the proposed model can be considered a crossover between the work of Gaunaa for the attached flow region and Hansen et al. *The model is compared qualitatively to wind tunnel measurements of a Risø B1-18 blade section equipped with deformable trailing-edge flap devices in the form of piezoelectric devices. Copyright © 2009 John Wiley & Sons, Ltd.*

Received 17 October 2007; Revised 17 December 2007; Accepted 28 January 2009

Notations

A_i, b_i	profile-specific constants for wake state variables
α	Incidence angle
$\alpha^{\beta}_{0,st}$	Equivalent shift in incidence due to a static β deflection angle
$\alpha^{\beta}_{0,dyn}$	Equivalent shift in incidence due to the first β derivative
α^{c}_{0}	Equivalent shift in incidence due to a cambered profile
α_0	Sum of $\alpha^{\beta}_{0,dyn}$, $\alpha^{\beta}_{0,st}$ and α^{c}_{0}
$\alpha_{3/4}$	Geometrical angle of attack at the three-quarter point
α_E	Effective geometric incidence using the unsteady wake effects from the shed vorticity
$\alpha_{o,E}$	Effective equivalent incidence using the unsteady wake effects from the shed vorticity
β	DTEF deflection angle
b	Airfoil half chord
c	Airfoil chord
C_{Do}	Drag coefficient at zero lift
$\Delta C_{D,DTEF}{}^{st}$	Stationary drag coefficient contribution from DTEF
$\Delta C^{dyn}{}_{D,DTEF}$	Dynamic drag coefficient contribution from the first and second derivative of the DTEF deflection.
$C_D{}^{dyn}$	Dynamic drag coefficient
$C_L{}^{P}$	The attached flow unsteady lift coefficient

*Correspondence to: Peter Bjørn Andersen, Risø-DTU, VEA, Roskilde, Denmark.
E-mail: peter.bjoern.andersen@risoe.dk

C_L^P,	Intermediate state variable; lift coefficient after the pressure time-lag is included
C_L^{st}	Stationary lift coefficient as function of incidence
C_L^{fs}	Fully separated stationary lift coefficient
$C_{L,\alpha}$	Lift coefficient slope for attached flow regime
C_L^{dyn}	Dynamic lift coefficient as function of incidence and DTEF deflection angle.
$\Delta C_{L,DTEF}{}^{st}$	Stationary lift coefficient contribution from DTEF
$\Delta C^{dyn}{}_{L,DTEF}$	Dynamic lift coefficient contribution from the first and second derivative of the DTEF deflection.
C_{Mo}	Moment coefficient at zero lift
C_M^{dyn}	Dynamic moment coefficient
$C_{M,DTEF}$	Dynamic moment coefficient contribution from DTEF
DTEF	Deformable Trailing-Edge Flap.
ε	Non-dimensional chordwise length parameter.
f^{dyn}	Dynamic separation point. Values range between one and zero.
f^{st}	Stationary separation point. Values range between one and zero.
H_{dydx}, H_y	Flap modeshape deflection integrals
k	Reduced frequency $k = \omega b/U$
τ_p, τ_b	Dynamic pressure-lift time lag and build-up/destruction time lag for the boundary layer
TE	Trailing Edge
U, U_0, **U**	Free-stream air velocity (U_x, U_y are coordinate components of U)
ω	Frequency
w	Three-quarter point downwash
w_β	Three-quarter point downwash contribution from DTEF
$w_{3/4}$	Three-quarter point downwash contribution from airfoil
x,y,z	Local coordinates used to describe DTEF
x_i,y_i,z_i	Indicial state variables for the wake history

Introduction

Adding a flap to a blade is a well-known method for changing the aerodynamic pressure distribution around the blade. Flap devices are used for noise and vibration reduction on rotorcrafts. Extensive works have been conducted in this area, and the authors refer to the review paper by Friedmann[1] for more details. For the purpose of this paper, the Deformable Trailing-Edge Flap (DTEF) is not intended as a classic plain flap that rigidly rotates around its hinge point, but, on the contrary, is represented by a continuous and smooth deformation of the airfoil trailing-edge (TE) part, specified through a non-linear deflection shape. Continuous research at Risø DTU National Laboratory for Sustainable Energy, Denmark involving this type of DTEF[2–6] showed that flow separation, noise and drag are reduced compared to a traditional rigid flap, and the potential fatigue load reduction by use of DTEF may be greater than for traditional pitch control methods. By mounting a number of DTEFs on a blade and enabling them to deflect independently local aerodynamic fluctuations due to unsteady inflow can be alleviated. Using a simple modal expanded blade model of a Vestas V66 wind turbine, Andersen *et al.*[3] found that the equivalent flapwise blade root moment could be reduced by 60% for inflow with 10% turbulence using a 7 m adaptive DTEF on the 33 m blade, subject to constant rotational rotor speed. More recent work involving a full multi-body aero-servo-elastic code[7] subject to more realistic conditions have showed load-reduction potentials of up to 48% of blade root moment in the flapwise direction.[8] In Figure 1, an airfoil with DTEF is shown with the DTEF in three different positions. Based on prior results,[6] the optimal DTEF length was 10% of the chord. The 10% was evaluated on high-control authority weighted against a small actuation cost and minor increase in airfoil drag. The notation connected to the airfoil geometry is shown in Figure 1, where AOA is the angle of attack or incidence of the incoming flow to the undeformed DTEF, β is the angle from the point where the DTEF is fixed on the non-deformable part of the airfoil to the TE positive towards the pressure side. The free-stream air velocity is denoted $\bar{U} = \sqrt{U_x^2 + U_y^2}$.

DOI: 10.1002/we

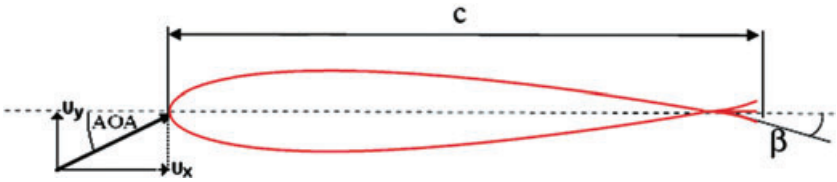

Figure 1. Notation of an airfoil equipped with DTEF. Three different positions of the DTEF are shown (1020 × 285 mm) (96 × 96 dpi)

All previous work investigating active load reduction using DTEF carried out at Risø DTU has used the aerodynamic model of Gaunaa,[5] which is an inviscid model. Therefore, the investigations have been confined to AOAs in the linear region, where effects of stall are not present. Because of the great load-reduction potential revealed previously, further investigations closer to and somewhat into the stalled region is needed. The present work contains an extension of the Beddoes–Leishman (BL)-type dynamic stall model,[9] as described by Hansen *et al.*,[10] with the static and dynamic effect of a DTEF. Another reference to a BL model can be found in the work of Larsen *et al.*[11] The model predicts the unsteady aerodynamic forces and moments on an airfoil section undergoing arbitrary motion in heave, lead-lag, pitch and TE flapping, and includes the effect of shed vorticity from the TE and the effect of an unsteady TE separation point. In the linear region, the model reduces to the inviscid model of Gaunaa. Therefore, the proposed model can be considered a crossover between the work of Gaunaa for the attached flow region and Hansen *et al.* for the separated flow region, and will make the aerodynamic forces a function of incidence and deflection of the flap (β). The model is not expected to handle large TE deflections, e.g. 30–45º; in fact, the deflection is limited to ±5º. The model is compared qualitatively with wind tunnel measurements of a Risø B1-18 blade section equipped with DTEF devices in form of piezoelectric devices, which is described in the work of Bak *et al.*[12] Many research groups around the world are investigating localized control surfaces. In the Netherlands, the main focus is on TE flaps at Delft University[13] and synthetic jets at ECN/University of Twente. In the USA, TE flaps and tabs are being investigated at Sandia National Laboratory in New Mexico and at UC Davis in California.[14] NTUA in Greece has focused their effort on TE flaps.[18]

Theoretical Model

The model consists of two parts: an inviscid and a viscous part. In the inviscid part, the airfoil is represented by its camberline, with the effect of the DTEF represented by a change in the camberline given by a deformation mode. The influence from the shed vorticity in the wake is described by a series of time-lags, as used by Hansen *et al.*[10] and Gaunaa,[5] in which the time-lag is approximated using an indicial function first outlined by Von Karman *et al.*,[16] making the practical calculation of the aerodynamic response numerically very efficient by use of Duhamel superposition. In the viscous part of the model, the dynamic behaviour of the TE separation is likewise modelled using a time-lag between pressure distribution and lift, and a time-lag for the separation point in the dynamic boundary layer. Using the same conditions as specified by Hansen *et al.*,[10] the TE separation is considered under stalled conditions.

This paper will deal with integrating the DTEF into the dynamic stall model by first describing the inviscid part of the DTEF model by Gaunaa,[5] then implementing this into an attached flow formulation, then a fully separated flow formulation and finally, the dynamics for the TE separation will be formulated.

DTEF Modelling Basics

Based on the work of Gaunaa, the lift, drag and moment can be found for an airfoil using a series of modeshapes that model an unsteady camberline. A single modeshape, illustrated in Figure 2, can be used to model the camberline of a DTEF undergoing unsteady deformations. Actuating the DTEF causes a change in the

DOI: 10.1002/we

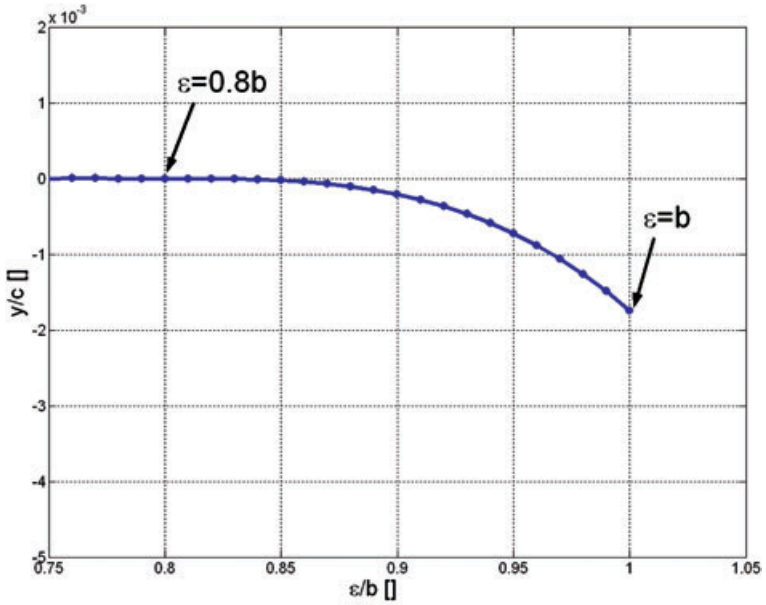

Figure 2. Modeshape (ε,y) used to model 1° DTEF deflection (β = +1°). The b mark the half-chord length (1219 × 883 mm) (96 × 96 dpi)

equivalent three-quarter downwash. This downwash is denoted $\boldsymbol{Q}$ in the work of Gaunaa, whereas the downwash will be called w_β in the present work, and only represent the DTEF contribution to the downwash. For steady conditions using a single deformation modeshape, w_β is given by

$$\frac{w_\beta}{\bar{U}} = -\frac{H_{dyd\varepsilon}}{2\pi}\beta - \frac{H_y}{2\pi\bar{U}}\frac{\partial\beta}{\partial t} \tag{1}$$

The deflection integrals H_y and $H_{dyd\varepsilon}$ are given by equations (2) and (3). Please note that the lower bound of 0.8 used in the integrals represents the start of a DTEF with a chordwise length of 10%, because x is a non-dimensional chordwise coordinate going from x = −1 at the Leading Edge (LE) to x = 1 at the TE

$$H_y = -2\int_{0.8}^{1} \frac{y(x)\sqrt{1-x^2}}{x-1}\,dx \tag{2}$$

$$H_{dyd\varepsilon} = -2\int_{0.8}^{1} \frac{\frac{\partial y}{\partial \varepsilon}(\varepsilon(x))\sqrt{1-x^2}}{x-1}\,dx \tag{3}$$

The w_β is a useful quantity for finding the DTEF contribution to lift, drag and moment, which has been derived by Gaunaa and shown in the Appendix for the simple one modeshape representation of a DTEF camberline. In some cases, empirical data for the DTEF is known, e.g. from wind tunnel measurements. It is possible to introduce the empirical term $\Delta C_{L,\mathrm{DTEF}}{}^{st}$ by replacing the theoretical H_{dydx}. The downwash (w) of equation (1) can be represented using equivalent incidence angles

$$\begin{aligned} \alpha^{\beta}_{0,st} &= \frac{H_{dydx}}{2\pi}\beta \cong \frac{\Delta C_{L,DTEG}(\alpha^{c}_{0},\beta)}{C_{L,\alpha}} \cong \frac{\partial C_L}{\partial\beta}\Big/\frac{\partial C_L}{\partial\alpha}\beta \\ \alpha^{\beta}_{0,dyn} &= \frac{H_y}{2\pi\bar{U}}\frac{\partial\beta}{\partial t} \end{aligned} \tag{4}$$

DOI: 10.1002/we

where the term $C_{L,\alpha}$ represents the attached lift slope at zero DTEF deflection β. The term $\alpha_{0,st}{}^{\beta}$ is an equivalent incidence angle that is shifted because of a static β deflection angle. The variable $\alpha_{0,dyn}{}^{\beta}$ indicate the contribution from the first β derivative to w_β given by equation (1). Using equation (4), the overall lift offset represented by a shift in incidence (α_0) because of a cambered profile and the use of a DTEF becomes equal to equation (5).

$$\alpha_o = \alpha_{0,st}^{\beta} + \alpha_{0,dyn}^{\beta} + \alpha_0^c \tag{5}$$

The term $\alpha_0{}^c$ is the offset at zero lift because of a standard cambered profile.

Lift in Attached Flow Using the BL and DTEF Model

As in the original work of BL, a geometric angle of attack at the three-quarter point $\alpha_{3/4}$ will be formulated as

$$\alpha_{3/4} = \frac{w_{3/4}}{\bar{U}} \tag{6}$$

The three-quarter point downwash without the influence of a DTEF is given by the variable $w_{3/4}$. The effective geometric incidence (α_E) is found using the unsteady wake effects from the shed vorticity following Duhamel integral formulation. The profile has a camberline that is changing in time because of the added DTEF. As shown in equations (4) and (5), this is interpreted as a time-varying zero lift angle. The unsteady offset of incidence α_0 is called $\alpha_{0,E}$. The unsteady DTEF deflection angle (β_E) is based on the static DTEF deflection angle (β) using the same integral formulation.

$$\begin{aligned}
\alpha_E &= \alpha_{3/4}\left(1 - \sum_i A_i\right) + \sum_i x_i \\
\alpha_{0,E} &= \alpha_0\left(1 - \sum_i A_i\right) + \sum_i y_i \\
\beta_E &= \beta\left(1 - \sum_i A_i\right) + \sum_i z_i
\end{aligned} \tag{7}$$

The indicial state variables for the unsteady aerodynamics corresponding to each of the above is

$$\begin{aligned}
x_i &= x_i \cdot e^{-ds \cdot b_i} + A_i \alpha_{3/4}\left(1 - e^{-ds \cdot b_i}\right) \\
y_i &= y_i \cdot e^{-ds \cdot b_i} + A_i \alpha_0\left(1 - e^{-ds \cdot b_i}\right) \\
z_i &= z_i \cdot e^{-ds \cdot b_i} + A_i \beta\left(1 - e^{-ds \cdot b_i}\right)
\end{aligned} \tag{8}$$

where ds is given by equation (A3), and A_i and b_i are profile-specific constants. Common practice is to use the flat-plate response approximation given by Jones.[17] The unsteady lift for attached flow is rewritten to include the DTEF deflection given by the unsteady offset of incidence

$$C_L^P = C_{L,\alpha}(\alpha_E - \alpha_{0,E}) + \pi b \frac{\dot{\alpha}}{\bar{U}} \tag{9}$$

where higher order terms of heave motion have been neglected.

Lift in Stalled Flow with TE Separation

This work is based on a variation of the BL model developed at Risø DTU.[10] The original BL model deals with both LE vortex shedding and TE separation; however, LE eddy separation is not included in Hansen

DOI: 10.1002/we

et al.[10] and will be omitted here as well. The static flat-plate lift in a Kirchoff flow[18] with the DTEF (β) deflection angle is written as

$$C_L^{st}(\alpha)+\Delta C_{L,DTEF}^{st}(\alpha,\beta)=C_{L,\alpha}\left(\frac{1+\sqrt{f^{st}(\alpha,\beta)}}{2}\right)^2[\alpha-\alpha_0(\beta)] \tag{10}$$

The α_0 contains the static offset in incidence for a cambered profile plus the DTEF deflection. The term $\Delta C_{\mathrm{L,DTEF}}{}^{\mathrm{st}}$ represent the stationary DTEF contribution to the lift given by CFD or measurements in a wind tunnel. $C_{\mathrm{L},\alpha}$ is the slope of the linear region of attached flow at zero β. The f^{st} determines the steady separation point for the TE separation as defined in Figure 3. The flow is fully attached for f = 1 and fully separated for f = 0. Assuming that the static lift curve is given, the separation point can be determined as a function of incidence and DTEF deflection angle (β) by inversion of equation (10).

$$f^{st}=\left(2\sqrt{\frac{C_L^{st}(\alpha)+\Delta C_{L,DTEF}^{st}(\alpha,\beta)}{C_{L,\alpha}(\alpha-\alpha_0(\beta))}}-1\right)^2 \tag{11}$$

The separation point can not exceed the LE of the airfoil of the linear lift slope

$$C_{L,\alpha}=\max\left\{\frac{C_L^{st}(\alpha)}{\alpha-\alpha_0(\beta=0)}\right\} \tag{12}$$

It is assumed that the flow in the attached region follows the $C_{\mathrm{L},\alpha}$ slope. To handle variations in (α,β) exceeding the limits of equation (11), the separation point is defined as zero for (α,β) values exceeding equation (13).

$$\left|C_L^{st}(\alpha,\beta)\right|=\left|\frac{C_{L,\alpha}(\alpha-\alpha_0(\beta_{\max}))}{4}\right| \tag{13}$$

The lift coefficient for fully separated flow ($C_{\mathrm{L}}{}^{\mathrm{fs}}$) is given by equation (15)

$$C_L^{st}=C_{L,\alpha}(\alpha-\alpha_0)f^{st}+C_L^{fs}(1-f^{st}) \tag{14}$$

$$C_L^{fs}=\frac{C_L^{st}(\alpha)+\Delta C_{L,DTEF}^{st}(\alpha,\beta)-C_{L,\alpha}(\alpha-\alpha_0)f^{st}}{1-f^{st}}\ \text{for}\ f^{\mathrm{st}}\neq 1 \tag{15}$$

where $C_{\mathrm{L}}{}^{\mathrm{st}}$ indicate the static lift curve, $\Delta C_{\mathrm{L,DTEF}}{}^{\mathrm{st}}$ the static lift from DTEF and f^{st} the static separation point given by equation (11). Equation (15) becomes equal to the static lift for incidence and DTEF deflections beyond equation (13). For fully attached flow, Hansen *et al.*[10] states that equation (14) must be inserted into equation (15) to avoid dividing by zero. Consequently, the fully separated lift in the attached region yields

$$C_L^{fs}(\alpha,\beta)\rightarrow\frac{C_L^{st}(\alpha,\beta)}{2}\ \text{for}\ f^{\mathrm{st}}=1 \tag{16}$$

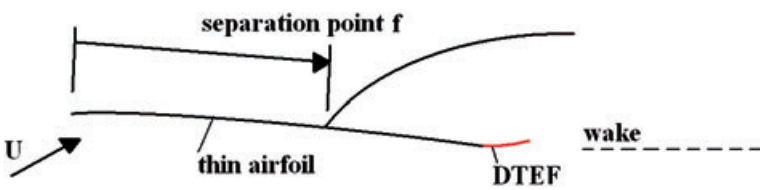

Figure 3. trailing edge separation point f defined in the Kirchoff flow past a flat plate (1079 × 275 mm) (96 × 96 dpi)

DOI: 10.1002/we

Hence, the lift for fully separated flow at low angles of attack is half the lift for fully attached flow. Figure 4 shows an example of a static lift curve represented by the interpolation equation (14). The step-by-step procedure for finding $C_{L,fs}$ and f^{st}.

Find the:

- incidence for zero lift for DTEF deflection at zero degree (α_0)
- maximum linear lift slope for zero DTEF deflection ($C_{L,\alpha}$)
- minimum and maximum limits for use of Kirchoff's static lift for flat plate flow by calculating the maximum incidence offset when using the DTEF, e.g. positive five degree DTEF deflection for maximum C_L and negative 5° DTEF deflection for minimum C_L. This is done to avoid dividing by zero in equation (15).
- separation point function f^{st} from equation (11) using the original lift curve for profile and DTEF contribution
- lift coefficient for fully separated flow (equation (15)), but using (equation (16)) for the attached flow region.

Dynamics of the TE separation

Two state variables in the BL model also implemented by Hansen *et al.*[10] are used to describe the dynamic behaviour of the TE separation. The separation is related to the pressure distribution over the airfoil, and the pressure is related to the lift on the airfoil; for a given lift, there is a certain pressure distribution with a certain separation point. It is assumed that there is a time-lag between the pressure and lift modelled as equation (17) and the dynamics of the boundary layer is modelled as equation (18).

$$C_L^{p'} = C_L^{p'} \cdot e^{\frac{-ds}{\tau_p}} + C_L^{P}\left(1 - e^{\frac{-ds}{\tau_p}}\right), \beta_E{}' = \beta_E{}' \cdot e^{\frac{-ds}{\tau_p}} + \beta_E\left(1 - e^{\frac{-ds}{\tau_p}}\right) \tag{17}$$

$$f^{dyn} = f^{dyn} e^{\frac{-ds}{\tau_b}} + f^{st'}\left(1 - e^{\frac{-ds}{\tau_b}}\right) \tag{18}$$

$$f^{st'} = f^{st}(\alpha, \beta), \text{ where } \alpha = \frac{C_L^{p'}}{C_{L,\alpha}}, \beta = \beta_E{}' \tag{19}$$

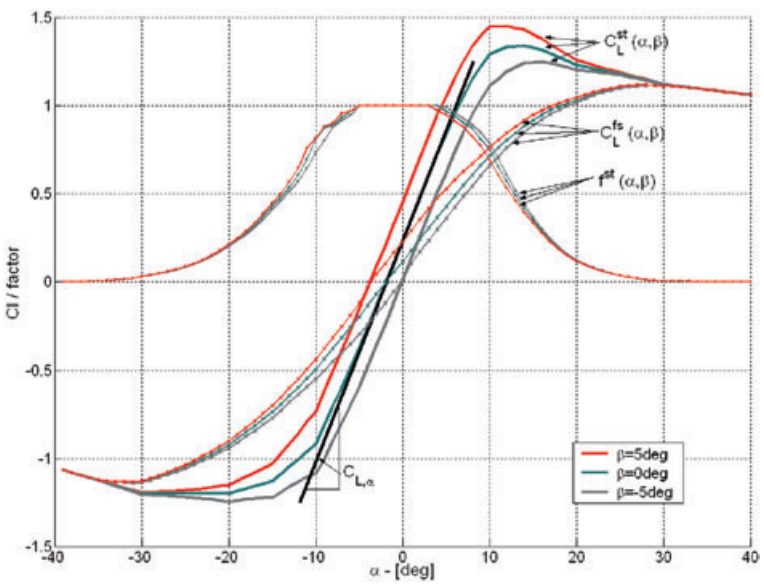

Figure 4. Static lift coefficient and TE separation curves for DTEF deflection (β) at –5°, 0° and 5°

DOI: 10.1002/we

The time constants τ_p and τ_b represent the time-lags for the dynamic pressure-lift lag and the dynamics in the build-up/destruction lag of the boundary layer. The $C_L^{P'}$ is a helping state variable containing the equivalent lift coefficient after the pressure time-lag has been included and β_E' is the effective pressure-lagged DTEF deflection angle. Using this semi-dynamic lift coefficient ($C_L^{P'}$) and effective DTEF deflection angle (β_E), the pressure-lagged separation point $f^{st'}$ is found using equations (11) and (19). The dynamic separation point is used in the linear interpolation between the full separation lift and the attached flow lift to find the overall dynamic lift with TE separation.

$$C_L^{dyn} = C_{L,\alpha}(\alpha_E - \alpha_{0,E}) f^{dyn} + C_L^{fs}(1 - f^{dyn}) + \pi b \frac{\dot{\alpha}}{\bar{U}} \tag{20}$$

Equation (20) does not include higher order terms given by equations (A6) and (A7), or higher order terms for heave motion. These terms have been considered and found to be an order of magnitude lower than the significant terms.

Drag

The unsteady drag is bounded to variations about a static drag curve provided as input to the model. The drag consists of three parts: *induced drag*, *viscous drag* and *DTEF contribution to drag* modelled as a change in incidence offset similar to the dynamic lift. A description of the *induced drag* is provided by Hansen *et al.*[10] The *viscous drag* is either calculated using CFD or measured in a wind tunnel. The suggested model assumes that the *DTEF drag contribution* scales with the dynamic separation point function (f^{dyn}). This assumption is not validated, but considered valid for the two extreme cases (fully attached flow and fully separated flow). The DTEF contribution to the geometric and effective incidence is included using the DTEF-specific helping variables $\alpha_{3/4,DTEF}$ and $\alpha_{E,DTEF}$ given in equation (21).

$$\begin{aligned} \alpha_{3/4,DTEF} &= \alpha_{3/4} - \left(\alpha_{0,st}^{\beta} + \alpha_{0,dyn}^{\beta}\right) f^{dyn} \\ \alpha_{E,DTEF} &= \alpha_E - \left(\alpha_{0,E} - \alpha_0^c\right) f^{dyn} \end{aligned} \tag{21}$$

The original dynamic drag C_D^{dyn} equation by Hansen *et al.*[10] is otherwise reused. Please refer to the paper by Hansen *et al.*[10] for details.

$$\begin{aligned} C_D^{dyn} &= C_D^{st}(\alpha_{E,DTEF}) + \Delta C_D^{ind} + \Delta C_D^{f^{dyn}} \\ \Delta C_D^{ind} &= \left(\alpha_{3/4,DTEF} - \alpha_{E,DTEF}\right) C_L^{dyn} \\ \Delta C_D^{f^{dyn}} &= \left(C_D^{st}(\alpha_{E,DTEF}) - C_{D,0}\right)\left(\left(\frac{1-\sqrt{f^{dyn}}}{2}\right)^2 - \left(\frac{1-\sqrt{f^{st}}}{2}\right)^2\right) \end{aligned} \tag{22}$$

It is assumed that the drag coefficient at zero lift ($C_{D,0}$) is unaffected by the DTEF.

Moment

The unsteady TE separation affects the moment through the travelling of the pressure centre because of separation. However, as for the drag, the present model binds the unsteady moment to variations about the static moment curve provided as input. The DTEF contribution to the dynamic moment ($C_{M,DTEF}$) (see equation (A8)) is added to equation (23) (please refer to the work of Gaunaa[5] for details).

$$C_M^{dyn} = C_M^{st}(\alpha_{E,DTEF}) + \Delta C_M^{f^{dyn}} + C_{M,DTEF} - \pi b \frac{\dot{\alpha}}{2\bar{U}} \tag{23}$$

Please refer to the paper by Hansen *et al.*[10] for details on the term $\Delta C_M^{f,dyn}$. A smaller term from the original BL model has been excluded, which was of no importance to the overall results.

DOI: 10.1002/we

Results

Figures 5–7 illustrate a comparison between the BL implementation by Hansen *et al.*[10] and the newly suggested dynamic stall model for both attached flow and stalled flow regimes without DTEF deflection. The DTEF deflection (β) is at its undeformed state at 0º. Arrows indicate the orientation of the loops in time. The incidence is changed harmonic at a reduced frequency of $k = \omega c/(2U\text{o}) = 0.15$. Figure 5 shows C_L as function of incidence angle for the original BL model and the suggested model using the same reduced frequency. The unsteady attached flow regime C_L comparison originates from an oscillatory pitching motion starting at incidence 6º and ending at 9º. The agreement between the present model and the BL is near perfect, the flat-plate steady-lift slope is included for comparison. The orientation of the unsteady loops follows what is normally seen in dynamic stall models and CFD. Figure 6 shows a similar comparison for the stalled regime starting at incidence 17.4º with maximum incidence at 19.5º. The unsteady loop area primarily stems from the dynamics of the boundary layer and the pressure-lift interaction part of both BL and the present model. A near-perfect match in unsteady lift is seen and the loop orientation is reversed for both models. Figure 7 shows C_D as function of incidence for the BL and the suggested model. Due to unsteady effects the drag coefficient nearly doubles compared to the steadystate case, which is substantial but also seen in CFD calculations.[16] The overall purpose for showing these figures is to illustrate the near-perfect agreement between the original implementation of the BL model suggested by Hansen *et al.*[10] and the model presented in this paper.

Figures 8 and 9 illustrate that the lift for the suggested dynamic stall model operates in agreement with the measurements performed in the Velux wind tunnel. Full lines show the measured ΔC_L loops from Velux described by Bak *et al.*[12] Lift values are shifted, so $\Delta C_\text{L} = 0$ for $\beta = 0$º. Dotted lines represent the presented model. The DTEF deflection β ranges from −3º to 1.97º for reduced frequency $k = \omega c/(2U\text{o}) = 0.081$, for $\beta =$ −2.8º to 1.3º $k = 0.181$ and finally for $\beta = -2$º to 0.76º $k = 0.518$. Arrows indicate the orientation of the loops in time. For the quasi-steady case, the lift measured in the wind tunnel is used directly in the model; unsteady effects are given by the present model, which match the dynamic lift loops measured in the wind tunnel well for the reduced frequencies and amplitudes used. For incidence angle at 4.6º, there is a good agreement between measurements and this model, with the exception that for the highest reduced frequency, the measurements shows a slightly more open loop. For incidence at 18.5º in deep stall, the DTEF flapping motion creates loops

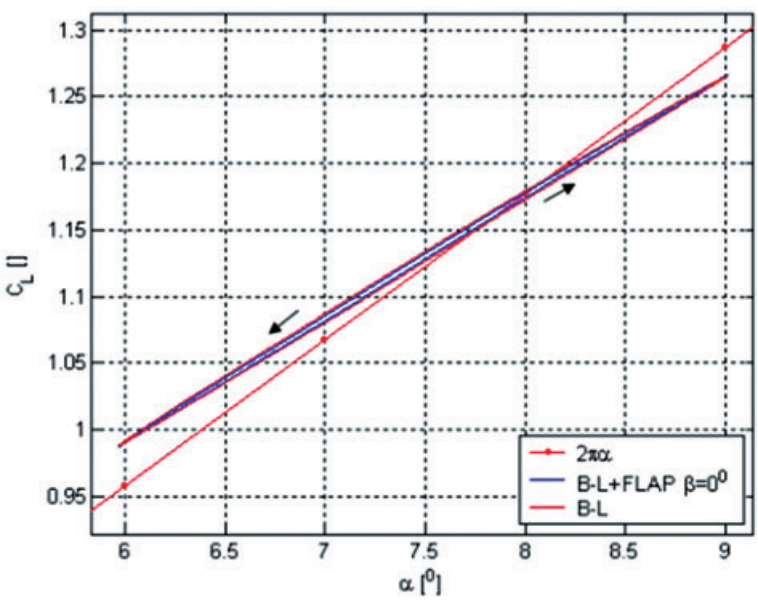

Figure 5. Unsteady lift coefficient comparison between the present model and the model by Hansen et al.[10] for the attached flow regime keeping constant undeformed DTEF (1021 × 800 mm) (96 × 96 dpi)

DOI: 10.1002/we

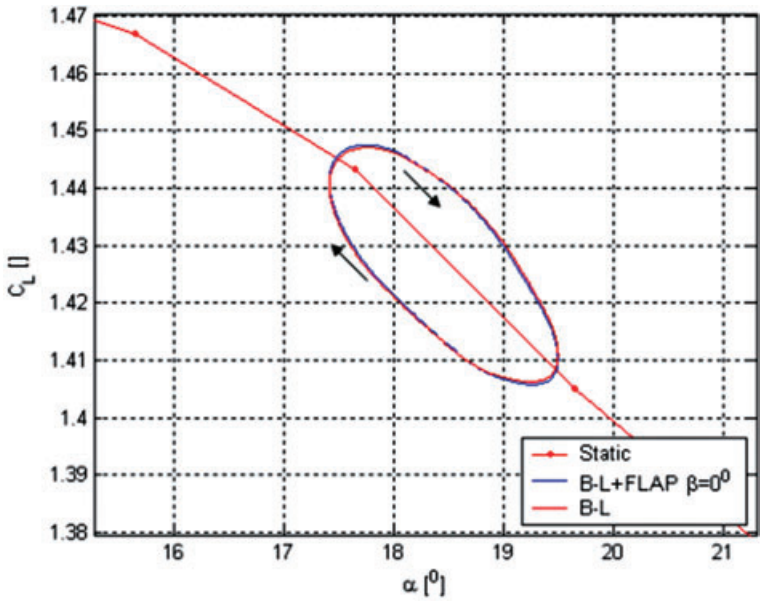

Figure 6. Unsteady lift coefficient comparison between the present model and the model by Hansen et al.[10] for the separated flow regime keeping constant undeformed DTEF (1035 × 800 mm) (96 × 96 dpi)

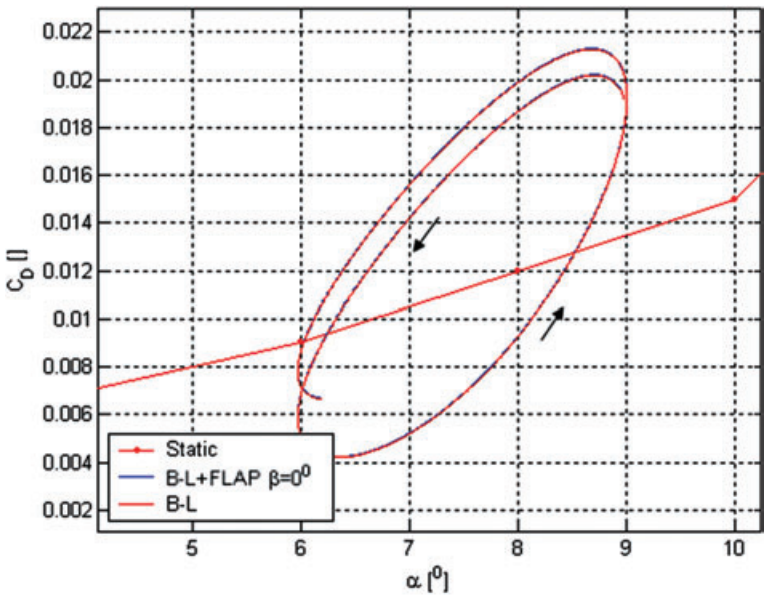

Figure 7. Unsteady drag coefficient comparison between the present model and the model by Hansen et al.[10] for the attached flow regime keeping constant undeformed DTEF (1064 × 838 mm) (96 × 96 dpi)

DOI: 10.1002/we

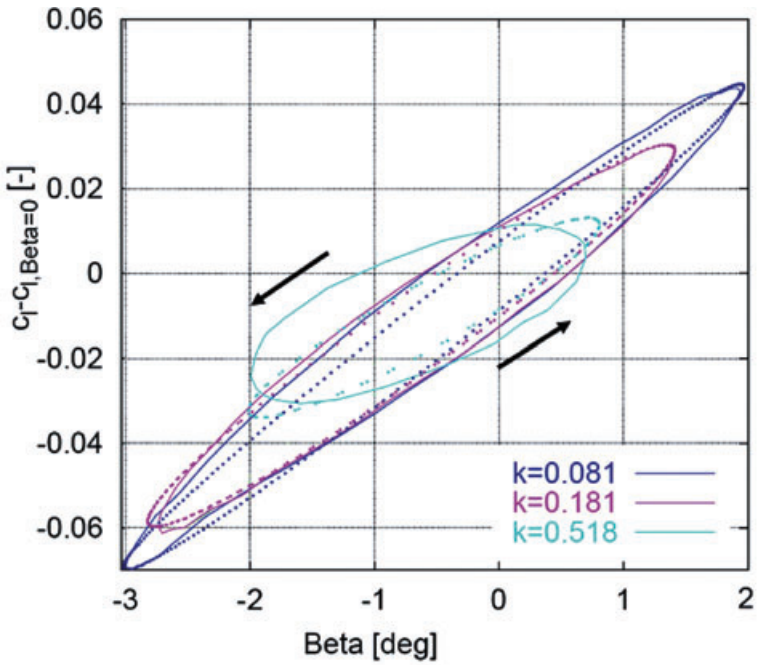

Figure 8. Unsteady lift coefficient comparison between the present model and measurements for attached flow regime using a constant incidence $\alpha = 4.6^{o}$ (203 × 176 mm) (96 × 96 dpi)

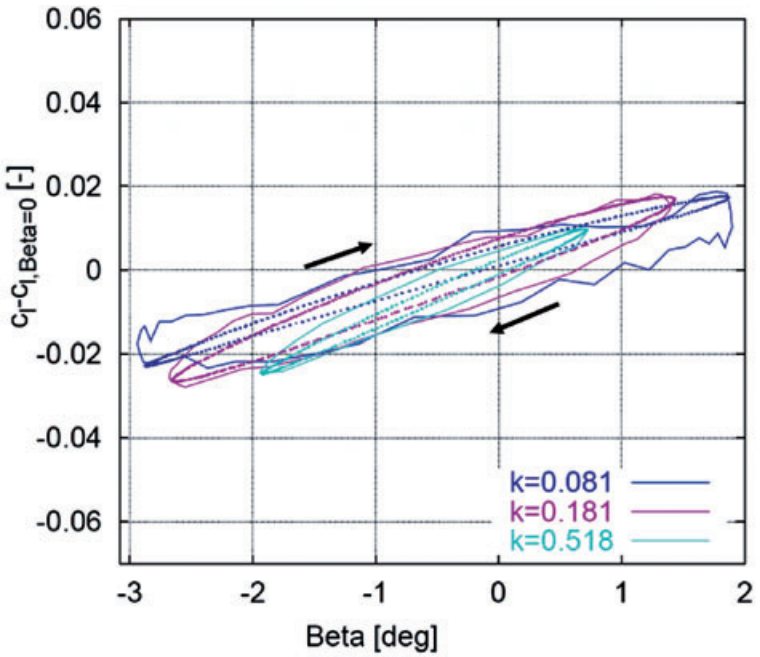

Figure 9. Unsteady lift coefficient comparison between the present model and measurements for separated flow regime using a constant incidence $\alpha = 18.5^{o}$ (1322 × 1105 mm) (96 × 96 dpi)

DOI: 10.1002/we

that are well captured by the model. Notice how the loop slope is becoming steeper for increased reduced frequency, a feature also seen in the measurements. The discrepancies in loop sizes between measurements and model at high reduced frequencies for both incidences may be linked with the wind tunnel corrections that are essentially quasi-steady phenomena. Although the Velux wind tunnel was not originally intended for blade measurements and the turbulence intensity is relatively high (around 1%), the measurements have shown a high level of reproducibility. As part of an inherent procedure, the corrected steady-state measurements are compared to CFD, literature data and previous measurements. Factors like tunnel blockage are included in the corrections of the raw measurements; however, it should be strongly emphasized that the present model only relies on steady-state measurements.

Figures 10–12 combine the pitching and flapping motion in phase where the reduced frequency is $k = \omega c/(2U\text{o}) = 0.1$. The amplitudes for the oscillatory pitching motion are 4º and 5º for the DTEF motion. The DTEF enlarge the pitching motion for Figures 10–12 because of the in-phase DTEF flapping motion. Figures 10–12 show three unsteady lift loops for the attached flow regime, stall and deep stall. Notably, the DTEF effect is decreased as the stall region is entered, and can be nearly disregarded for deep stall. Hence, the present model will not overpredict the potential of a DTEF when applied to an aero-elastic code simulating incidences outside the attached flow region.

Figures 13–15 show oscillatory pitching motion and DTEF motion in counter phase where the reduced frequency is $k = \omega c/(2U\text{o}) = 0.1$. The amplitudes for the oscillatory pitching motion are 4º and 5º for the DTEF motion. Figure 15 suggest that with the chosen pitching and DTEF deflection amplitudes in counter phase, the C_{M} loop slope at incidence angle of 4º can be removed, and the C_{L} loop shown in Figure 13 can be halved using the combined counter-phase DTEF deflection and pitching motion compared with the pure pitching motion.

The results shown are given by the suggested model using the DTEF measurements of static lift, drag and moment coefficients on a B1-18 profile as input. These figures illustrate the aerodynamic complexity of combining not only the pitching motion of a profile, but also adding a dynamic DTEF deflection motion. It should be noted that the unsteady part of drag and moment scales with the dynamic separation coefficient when actuated by the DTEF. This scaling causes the effect of using a DTEF to be zero in deep stall with regard to drag and moment; a better approach would be to extend the model to include the DTEF measurements for deep-stall scaling of drag and moment as done for the lift.

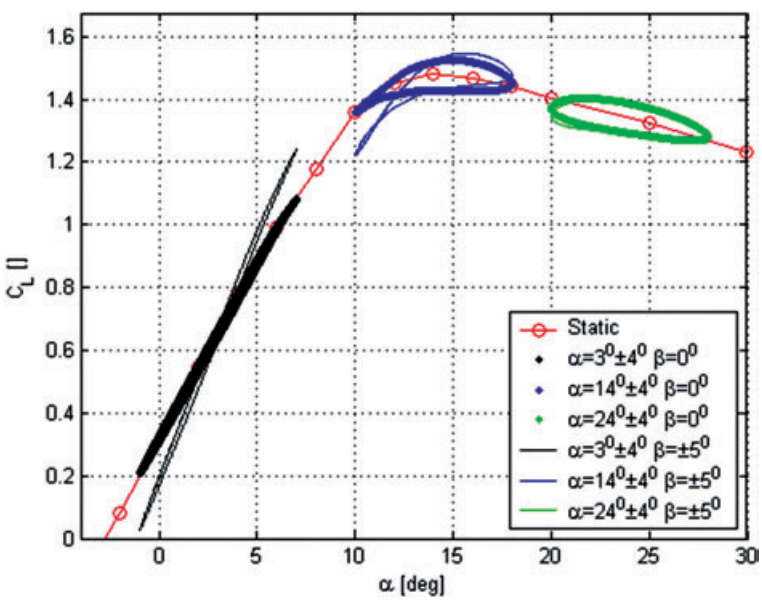

Figure 10. Unsteady C_L from in-phase pitching and DTEF oscillatory motion (1044 × 820 mm) (96 × 96 dpi)

DOI: 10.1002/we

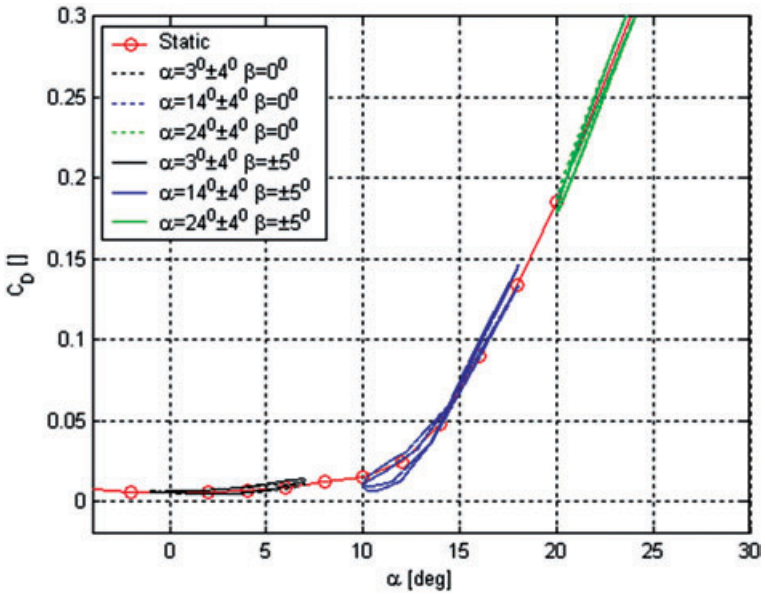

Figure 11. Unsteady C_D from in-phase pitching and DTEF oscillatory motion (1066 × 834 mm) (96 × 96 dpi)

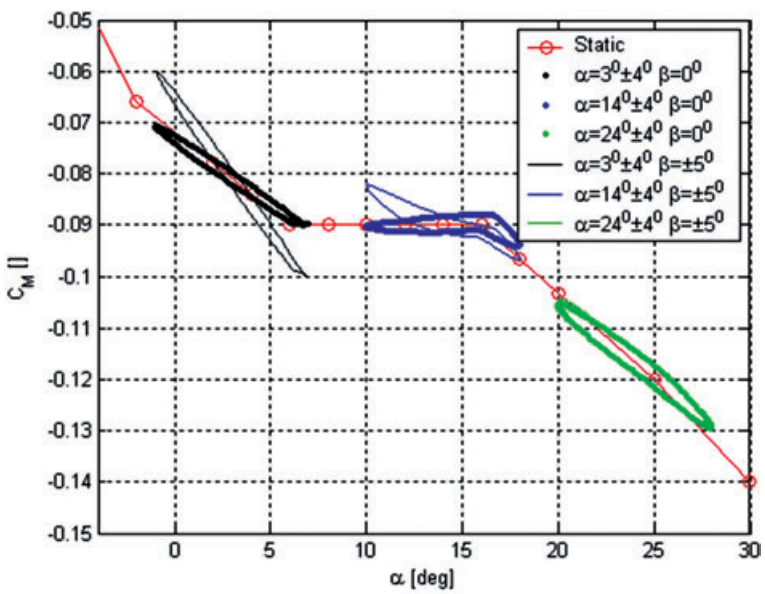

Figure 12. Unsteady C_M from in-phase pitching and DTEF oscillatory motion (1078 × 823 mm) (96 × 96 dpi)

DOI: 10.1002/we

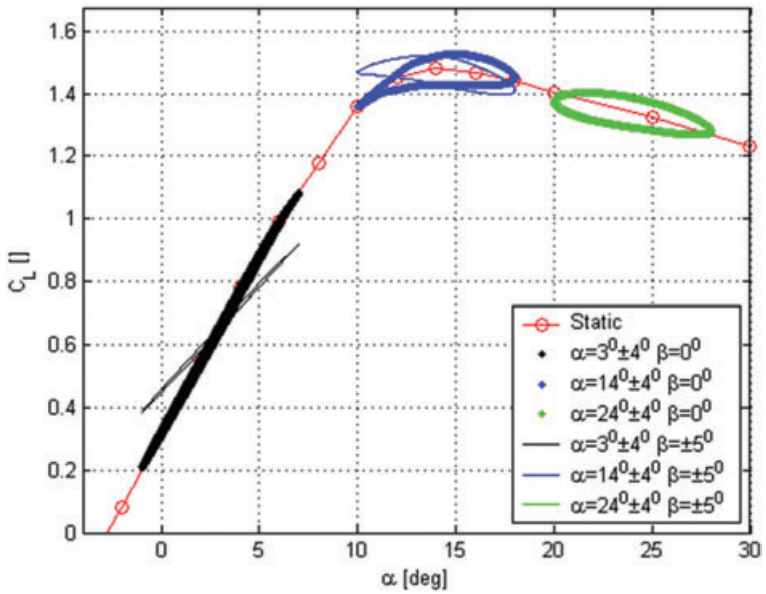

Figure 13. Unsteady C_L from counter-phase pitching and DTEF oscillatory motion (1049 × 828 mm) (96 × 96 dpi)

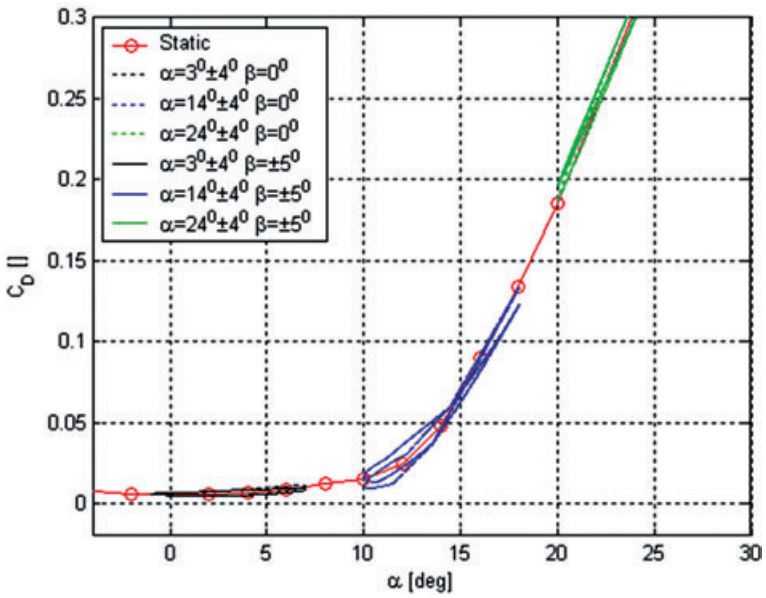

Figure 14. Unsteady C_D from counter-phase pitching and DTEF oscillatory motion (1067 × 839 mm) (96 × 96 dpi)

DOI: 10.1002/we

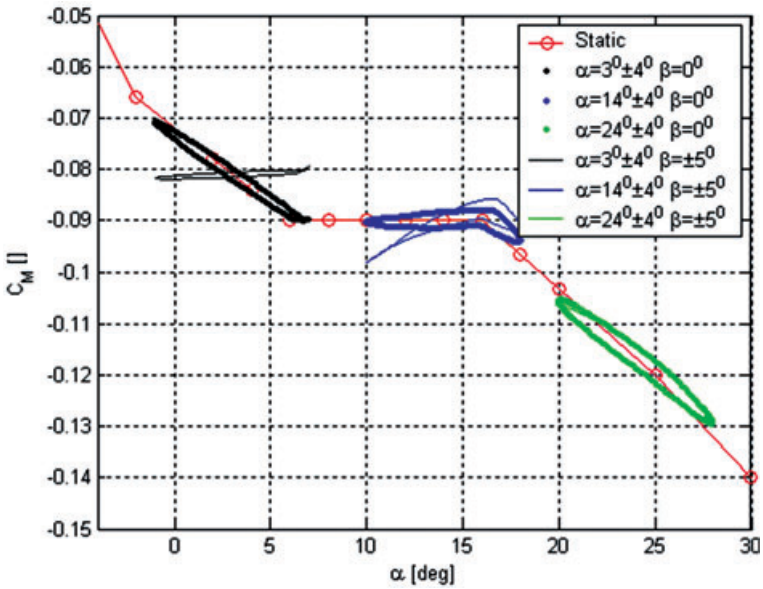

Figure 15. Unsteady C_M from counter-phase pitching and DTEF oscillatory motion (1066 × 827 mm) (96 × 96 dpi)

Conclusion

A dynamic stall model has been developed that predicts the unsteady aerodynamic forces and moments on an airfoil section undergoing arbitrary motion in heave, lead-lag, pitch and TE flapping. For zero DTEF deflections, the model becomes equivalent to the original implementation of the BL model by Hansen *et al.*[10] When actuating the DTEF, the model becomes equal to the Gaunaa model[5] in the attached flow region excluding some higher order terms that is part of the original Gaunaa model. For the separated flow region, the model becomes a crossover between the two models when using the DTEF. The dynamic lift in both stalled and attached region show good agreement with the measurements performed in the Velux tunnel.

References

1. Friedmann PP. Rotor–wing aeroelasticity: current status and future trends. *AIAA Journal* 2004; **42**: 10.
2. Abdallah I. Advanced load alleviation for wind turbines using adaptive trailing edge geometry: sensoring techniques. MSc Thesis Project. 13 July 2006, Technical University of Denmark, Department of Mechanical Engineering, Section of Fluid Mechanics, 2006.
3. Andersen PB, Gaunaa M, Bak C, Buhl T. Load alleviation on wind turbine blades using variable airfoil geometry. In *Proceedings of the 2006 European Wind Energy Conference and Exhibition*, Athens, Greece, 27 February–2 March 2006. European Wind Energy Association: Brussels, 2006.
4. Buhl T, Gaunaa M, Bak C. Potential load reduction using airfoils with variable trailing edge geometry. *Journal of Solar Energy Engineering* 2005; **127**: 503–516.
5. Gaunaa M. Unsteady 2D potential-flow forces on a thin variable geometry airfoil undergoing arbitrary motion. *Risø-R-1478*, Risø, Roskilde, Denmark, June 2004.
6. Troldborg N. Computational study of the Risø-B1-18 airfoil with a hinged flap providing variable trailing edge geometry. *Wind Engineering* 2005; **29**(26): 89–114.
7. Larsen TJ, Hansen AM. *How 2 HAWC2, the User's Manual*. Risø-R-1597 (ver. 3-1)(EN), 2007.

DOI: 10.1002/we

8. Andersen PB, Henriksen LC, Gaunaa M, Bak C, Buhl T. Integrating deformable trailing edge geometry in modern Mega-Watt wind turbine controllers. In *Scientific Proceedings of the 2008 European Wind Energy Conference*, Brussels.
9. Leishman JG, Beddoes TS. A generalized model for airfoil unsteady aerodynamic behavior and dynamic stall using indicial method. In *Proceedings of the 42nd Annual Forum of the American Helicopter Society*, Washington D.C., June 1986.
10. Hansen MH, Gaunaa M, Madsen HAA. A Beddoes–Leishman type dynamic stall model in state-space and indicial formulations. *Risø-R-1354*, Risø, Roskilde, Denmark, June 2004.
11. Larsen JW, Nielsen SRK, Krenk S, Dynamic stall model for wind turbine airfoils. *Journal of Fluids and Structures* 2007; **23**: 959–982.
12. Bak C, Gaunaa M, Andersen PB, Buhl T, Hansen P, Clemmensen K, Moeller R. Wind tunnel test on wind turbine airfoil with adaptive trailing edge geometry. Paper for conference *AAIA-2007-1016*, Reno, NV, 2007.
13. Barlas T, van Kuik GAM. State of the art and prospectives of smart rotor control for wind turbines. In *Journal of Physics 5, 2007 2nd EWEA, EAWE The Science of Making Torque from Wind Conference*, DTU, 28–31 August 2007.
14. Van Dam CP, Chow R, Zayas JR, Berg DA. Computational investigations of small deploying tabs and flaps for aerodynamic load control. In *Technical Paper Journal of Physics 5, 2007 2nd EWEA, EAWE The Science of Making Torque from Wind Conference*, DTU, 28–31 August 2007.
15. Voutsinas S. Aeroelastic modeling of the active flap concept for load control. In *Scientific Proceedings of the 2008 European Wind Energy Conference*, Brussels, 2008.
16. von Karman TH, Sears WR. Airfoil theory for non-uniform motion. *Journal of the Aerodynamical Science* 1938; **5**: 379–390.
17. Jones RT. The unsteady lift of a wing of finite aspect ratio. *Tech. Rep. 681*, NACA Report, 1940.
18. Thwaites BE. *Incompressible Aerodynamics*. Cambridge University Press: Cambridge, 1961.

Appendix: Attached Flow Equations for Deformable Trailing-edge Flaps

In the following, a simplified version, including only the influence of the flap from the original Gaunaa model,[5] will be given. Kelvin's theorem states that the change in global circulation for an unsteady 2D potential flow solution is zero. A step change in DTEF will cause a change in the circulation around the profile, in order to keep the global circulation constant vorticity of equal magnitude, but opposite sign is shed at the trailing edge and convected away from the airfoil by the free stream. The effective three-quarter downwash termed *QC* in the work of Gaunaa will be termed w_β^{E} in this paper. Von Karman *et al.*[16] showed how the effect of an unsteady wake can be added to the three-quarter downwash using the indicial function concept equation (A1). The aerodynamic state variable y_i is given by equation (A2).

$$w_\beta^E = w_\beta\left(1-\sum_i A_i\right)+\sum_i y_i \tag{A1}$$

$$y_i = y_i \cdot e^{-ds\cdot b_i} + A_i w_\beta\left(1-e^{-ds\cdot b_i}\right) \tag{A.2}$$

The non-dimensional step *ds* is given by equation (A3)

$$ds = \frac{1}{b}\int_t^{t+\Delta t} \bar{U}(t')\,dt' \tag{A.3}$$

A_i and b_i are profile specific constants. Common practice is to use the flat-plate approximation provided by Jones.[17]

Once the effective three-quarter downwash (w_β^{E}) is known, the DTEF contribution to the normal ($C_{\mathrm{N,DTEF}}$) and tangential force ($C_{\mathrm{T,DTEF}}$) can be found along with the contribution to the moment ($C_{\mathrm{M,DTEF}}$). See the following equations:

DOI: 10.1002/we

$$C_{N,DTEF} = \frac{b}{\pi \bar{U}^2}\left(\ddot{\beta} F_{y,2} + \dot{\beta} F_{dyd\varepsilon,2}\bar{U} - \beta F_{dyd\varepsilon,2}\dot{U}_x\right) + 2\pi \frac{w_\beta^E}{\bar{U}} \tag{A4}$$

$$\begin{aligned} C_{T,DTEF}\cdot\bar{U}^2 = \Bigg| & \frac{\pi}{2}\left(2w^E_{\cdot fullflap} - \dot{\alpha}b + \frac{\dot{U}_y}{2\pi}\left(K_{dydx,1} + H_{dydx,1} + \beta K_{dydx,2} + \beta H_{dydx,2}\right) + \frac{\dot{\beta}}{2\pi}\left(K_{y,2} + H_{y,2}\right)\right)^2 \\ & -\frac{\pi}{2}\left(2w^E_{noflap} - \dot{\alpha}b + \frac{\dot{U}_y}{2\pi}\left(K_{dydx,1} + H_{dydx,1}\right)\right)^2 \\ & +2b\beta\cdot TI1_2\left(\dot{U}_y - ab\ddot{\alpha}\right) \\ & +\frac{b}{\pi}\ddot{\beta}\left(TI2_{2,1} + \beta\cdot TI2_{2,2}\right) \\ & -\frac{b}{\pi}\dot{U}_y\beta\left(TI3_{2,1} + TI3_{1,2} + \beta\cdot TI3_{2,2}\right) \\ & +\frac{b}{\pi}\bar{U}\dot{\beta}\cdot TI3_{2,1} \\ & +b^2\ddot{\alpha}\beta\cdot TI4_2 \\ & -2\bar{U}\left[w^E_{fullflap}\left(TI5_1 + \beta TI5_2\right) - w^E_{noflap}\cdot TI5_1\right] \\ & -b\bar{U}\dot{\alpha}\beta\cdot TI6_2 \\ & +\frac{\bar{U}^2}{\pi}\beta\left(TI8_{2,1} + TI8_{1,2} + \beta\cdot TI8_{2,2} - H_{dydx,1}\cdot TI7_2 - H_{dydx,2}TI7_1 - \beta\cdot H_{dydx,2}TI7_2\right) \\ & +\frac{\bar{U}}{\pi}\dot{\beta}\left(TI9_{2,1} + \beta\cdot TI9_{2,2} - H_{y,2}\left(TI7_1 + \beta\cdot TI7_2\right)\right) \end{aligned} \tag{A5}$$

$$C^{dyn}_{N,DTEF} = \frac{b}{\pi\bar{U}^2}\ddot{\beta}F_{y,2} + \frac{b}{\pi\bar{U}}\dot{\beta}F_{dyd\varepsilon,2} \tag{A6}$$

$$\begin{aligned} C^{dyn}_{T,DTEF} = \Bigg| & \frac{\pi}{2\bar{U}^2}\left(\frac{\dot{\beta}}{2\pi}\left(K_{y,2} + H_{y,2}\right)\right)^2 \\ & +\frac{b}{\pi\bar{U}^2}\ddot{\beta}\cdot TI2_{2,1} \\ & +\frac{b}{\pi\bar{U}}\dot{\beta}\cdot TI3_{2,1} \\ & +\frac{\bar{1}}{\pi\bar{U}}\dot{\beta}\left(TI9_{2,1} - H_{y,2}TI7_1\right) \end{aligned} \tag{A7}$$

DOI: 10.1002/we

$$
C_{M,DTEF}\bar{U}^2\pi = \left|\begin{array}{l}
b\dot{U}_x\beta(G_{dydx,2} - a\cdot F_{dydx,2}) \\
+\bar{U}^2\beta(F_{dydx,2} + H_{dydx,2}) \\
-b\bar{U}\dot{\beta}(G_{dydx,2} - a\cdot F_{dydx,2}) \\
+\bar{U}\dot{\beta}\cdot F_{y,2} \\
0.5\pi\dot{\beta}\cdot H_{y,2} \\
-b\ddot{\beta}(G_{y,2} - a\cdot F_{y,2}) \\
+2\pi^2\bar{U}(0.5+a)\left(w_\beta^E\right) \\
-C_{N,DETEG}\cdot\pi\bar{U}^2
\end{array}\right. \tag{A8}
$$

For the constants *TI*1, *TI*2, *TI*3, *TI*4, *TI*5, *TI*6, *TI*7, *TI*8, *TI*9, *F*, *G* and *K*, please refer to Gaunaa.[5] The notation $\dot{()}$ represents the derivative with respect to time.

DOI: 10.1002/we